METHODS OF IDENTIFICATION
OF COUPLED VORTEX STRUCTURES IN MOTION

Václav Něnička, Václav Tesař, Jiří Šonský
Institute of Thermomechanics v.v.i., Academy of Sciences of the Czech Republic, Prague

Abstract

Compared with the general character of "laser knife" sections through jets in meridian plane, which agree with the expectations, the cross sections (perpendicular to the jet axis) reveal surprising complexity. In particular, in the authors' experiment, a jet at $Re = 10\ 200$ impinging on a transparent flat plate positioned at $h/D = 2.5$ was illuminated by laser light sheet at a distance $0.25\ h$ from the nozzle exit. Images of the light scattered on water droplet particles have shown in the mixing region (outside the jet core) vortical motions strongly suggesting the twisting and braiding movements of hair when a plait hairdo is made. Similar braiding movements observations were made — especially in flowfields associated with mixing of fluids — by other authors who for the explanation have recently developed a number of methods for description of such processes. In particular, we have found useful the theory that evaluates the measure of entanglement in fluids by the close comparison with the mathematical group of braiding movements. While these authors apply this theory on artificial, computer-generated data sets, our aim is to apply this approach on the accumulated experimental data on the coupled vortex objects, identified by the method of image processing by local correlation coefficient evaluations in sub-images interrogated in a sequence.

1. Introduction

Vortical structures occur in fluid flows due to hydrodynamic instability. They gradually grow in size and lose their initial coherence, disappearing finally in the surrounding chaotic turbulence. Authors identified them and studied the dynamics of their evolution in an experimental investigation of an impinging submerged air jet, in the facility shown in Fig. 1.

Impinging jets are fluid flows of particular importance in engineering applications — they p[osses a special position in heat and mass transfer convective processes since they can achieve the highest obtainable transfer rates between a fluid and a solid surface (e.g., Tesař and Trávníček [1]). The limiting factor of decisive importance for the heat and mass transfer is actually a thin fluid layer held on the impingement surface by fluid viscosity. The transfer across it is, because of its immobility, only by conduction transport. This is (especially in gases) very ineffective so that the wall layer, however thin, causes the substantial proportion of the overall resistance to the transfer. There were many attempts by various researchers to destroy the conductive layer or at least suppress its influence by oscillating the nozzle flow. The results were sometimes positive, sometimes negative and often indifferent. The reason for the lack of success was poor utilisation of the power applied for generation of the pulsation. The power was often spent on generation and driving of the instability vortices. The pulsations produced in the nozzle may not even reach to the impingement surface.

Obviously, it is essential for further progress in enhancement of the transfer processes to obtain more information about the vortices and their generation. This is not a new idea. Unfortunately, the processes are complex and obtaining clear understanding is difficult. All aspects of the vortex formation and of their role in impinging jets are
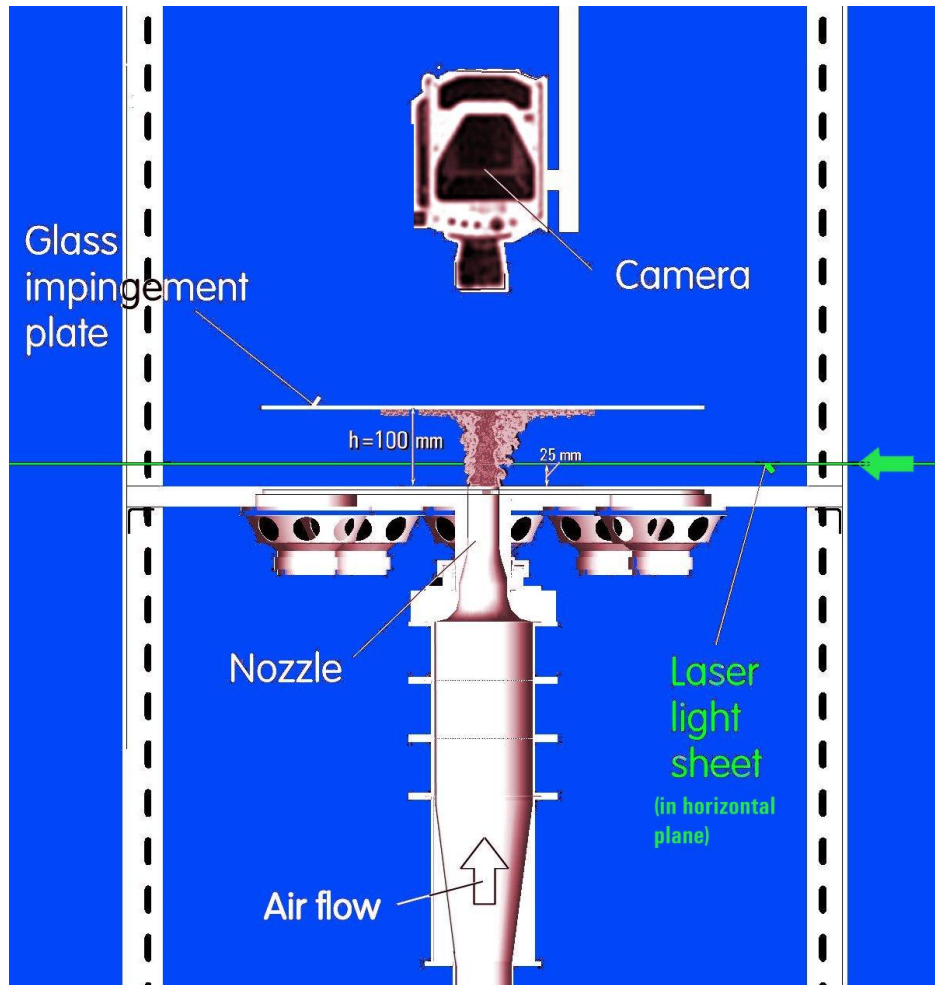
Fig. 1 The experimental facility, shown in meridian section. The air jet generated in the nozzle impinges upon the glass plate. The apparent cross section through the jet is made by the "laser knife" at the distance $0.25\,h$ from the nozzle and is recorded by the camera hidden behind the impingement plate.

therefore so far not fully elucidated. An example of the difficulties has been the slow progress in understanding the off-axis maxima phenomenon. It is a well known fact that if the nozzle is positioned at a small relative distance from the impingement wall (such as, e.g., equal to about 2 nozzle exit diameters), measurements of the local heat or mass transfer rate on the impingement wall exhibit strange maxima away from the stagnation point (the point on the intersection of the nozzle axis with the surface) [2]. These maxima, according to general consensus, are caused by the vortical motions. The details, however, of the mechanism generating these maxima are as yet not fully understood.

In fact, the very theory of hydrodynamic instabilities that are in the background of observed vortical motion is quite complex and so far not completely developed. This is why their investigations have to be mainly performed by laboratory experiments. In fact, even extracting useful knowledge from these experiments is rather difficult [3, 4, 5, 6]. The main problem encountered is the unsteady nature, fast motion of the instability structure and fast variation of its shape. The vortical motions that evolve have rather vague and indistinct, irregular boundaries, making precise location of the vortices uncertain. If a sequence of structures that appear in succession at a location in the

flowfield is watched, it becomes immediately apparent that all the structures are not identical to their predecessor. In such situations, it seems reasonable step to evaluate the general features by averaging. This should remove the idiosyncrasies of individual objects. Such an averaging, however, is not easy. Even though the structures seem to be appearing periodically, their periodicity is only approximate. An individual structure usually appears at a phase shift randomly varying relative to the ideal period. This makes identification of a structure - and its inclusion into the averaging procedure - quite uncertain. A particularly troublesome problem is the necessity to separate this phase jitter from the superimposed fully chaotic turbulence, by which the structures are surrounded and within which they finally fully disappear. In the discussed experiments, the phase jitter was eliminated by triggering the structure formation by a signal applied in the nozzle exit. Generation of this signal is the reason why there are the loudspeakers visible in Fig. 1.

2. Experiment

The investigated air jet was generated in a nozzle of $d = 40$ mm exit diameter. The nozzle exit was located in the centre of a large (800 mm x 800 mm) horizontal plate, perpendicular to the jet axis. Aerodynamic properties of the nozzle were evaluated in preliminary experiments using the basic ideas presented in reference [7]. The jet impinged upon the planar surface positioned above the nozzle exit at a distance $h = 100$ mm, i.e. at relative height equal to 2.5 nozzle diameter D. The blower that supplied the air flow into the nozzle was driven by an adjustable-speed electric motor. From the blower the air flow passed through a settling chamber (below the nozzle in Fig. 1), which was inside provided with two flow stabilising sieves placed in series. The variation of the blower speed made possible adjusting the Reynolds numbers of the jet in the range of the order $1 .10^3 - 10 .10^3$. Most experiments were actually made near the upper limit of this range, at Reynolds numbers near to $10 .10^3$. Visualisation of the jet was made possible by addition of water mist particles produced in the fog generator, placed upstream from the driving blower.

The triggering of the vortical structure generation was made by the electronic circuit designed and built by M. Pavelka [28]. The idea was to apply harmonic pressure action in the eight waveguide exits. The waveguides are arranged in the Catherine-wheel manner around the nozzle, the harmonic pressure variations was produced by standard loudspeakers of 100 W nominal electric input power (actual power level applied was lower by several decimal orders of magnitude). The circuit made possible generating azimuthal variations of pressure in the nozzle exit producing two helical vortices on the opposite sides of the jet — by applying the progressive phase delays in the individual loudspeakers [11, 12, 13]. Extraordinary feature of helical instabilities is their reputed capability to be capable of producing reverse spectral transport of energy towards larger wavenumbers [14]. The frequency of the triggering signal was set on the basis of a fit into the data from preliminary tests in which the natural frequency was investigated of appearance of vortices – and averaging the results. The dependence of the mean values on the Reynolds number as presented in [11] but later corrected by using measured [29] convective velocity rather than simply the bulk velocity in the nozzle exit, was found to follow the mixing-layer instability law of constant
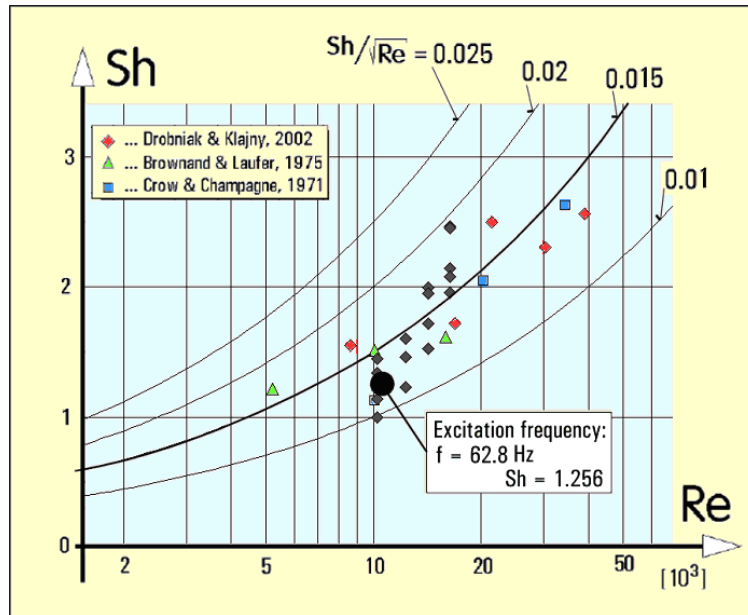
$$Sh / \sqrt{Re}$$

...(1)

Fig. 2 Dependence of Strouhal number Sh of natural instabilities in the mixing layer (computed from the vortex comvection velocity w_c) on Reynolds number Re computed, as usual, from the the nozzle exit velocity w_e). This diagram was used to adjust the excitation frequency.

In particular, with the nozzle exit velocity w_e = 4 m/s (at Reynolds number computed from the bulk velocity Re = 10.1 10^3) the natural frequency was f = 62.8 Hz, so that the Strouhal number (computed from the convection velocity w_c = w_e/2 = 2 m/s) was Sh = 1.256 so that the expression from eq. (1) was

$$ Sh / \sqrt{Re} = 0.0125 $$

... (2)

 - a value (cf. Fig. 2) that agrees very well with the existing data of other investigators, cf. [8]. [9], [10].

3. Images

The jet was visualised by scattering of the laser light on the mist particles illuminated by the "laser knife" – a sheet of laser light produced by cylindrical laser optics. The images of the scattered light were captured by a digital camera positioned above the impingement plate. The camera lens axis oriented perpendicularly to the light sheet. which in this case was transparent. The camera recorded the intensity of the scattered light in a particular location of the image frame. Essentially, this represented an information about the local concentration of the mist particles – though this information was not extracted from the pictures, which were merely used to observe the motions of particular features between subsequent frames. The laser a diode-pumped solid state green-light (wavelength 532 nm) Nd:YAG laser DPGL-2200L-45 supplied by Shanghai Uniwave Technology Ltd. Its maximum output power is 200 mW. The optics generated the light sheet of fan angle 45° and guaranteed width < 5 mm at a 5 m distance.
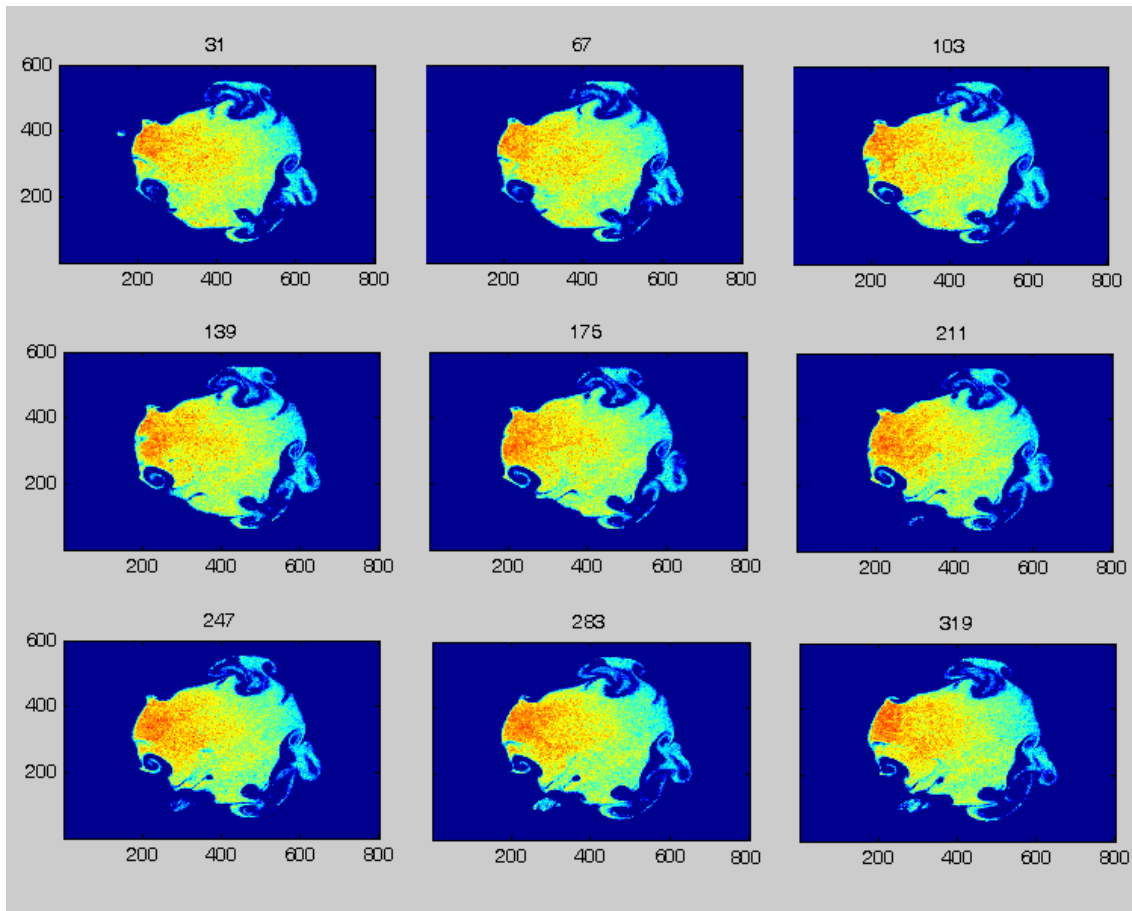
Fig. 3 Typical examples of cross-section images recorded in the same phase of the harmonic triggering. This sample of nine images demonstrates the performance of triggering signal generator designed and built by Mr. M. Pavelka. Intensity of scattered light corresponds to the local density of water droplets concentration.

The camera used to record the visualization images was Phantom v7.3 , supplied by Vision Research Inc., continuously recording on 14-bit monochrome SR-CMOS sensors giving 800 x 600 pixels resolution. The top speed of 6 688 frames per second was not utilised in the present case (lower speed makes possible recording less illuminated objects). In the example series of pictures of unexcited jet presented in Fig. 11, the frame acquisition speed was 100 frames per second. The original monochrome picture outputs were various levels of grey colour. The entrained outer air containing no mist droplets appeared black so that ideally the numerical value stored for the corresponding pixel of the image should be 0. There is, however, always some inevitable light dispersion inside the test space and also the absorbance of the background (which was a black textile curtain) was not perfect, so that the minimum values were higher. On the other hand, no pictures contained the full 14 bit white colour extreme. As a result, instead of the theoretical 14 bit range of the grey values from 0 to 16 384, in practical situations the pixel values were all in a much more narrow range. For the data processing, the values were adjusted so as to make the lowest value exactly zero. Typically, after the shift, the highest values were typically near to 9 000. To facilitate visual inspection of the images, the levels of grey were actually replaced by a false colour using an assignment function, an example of which is
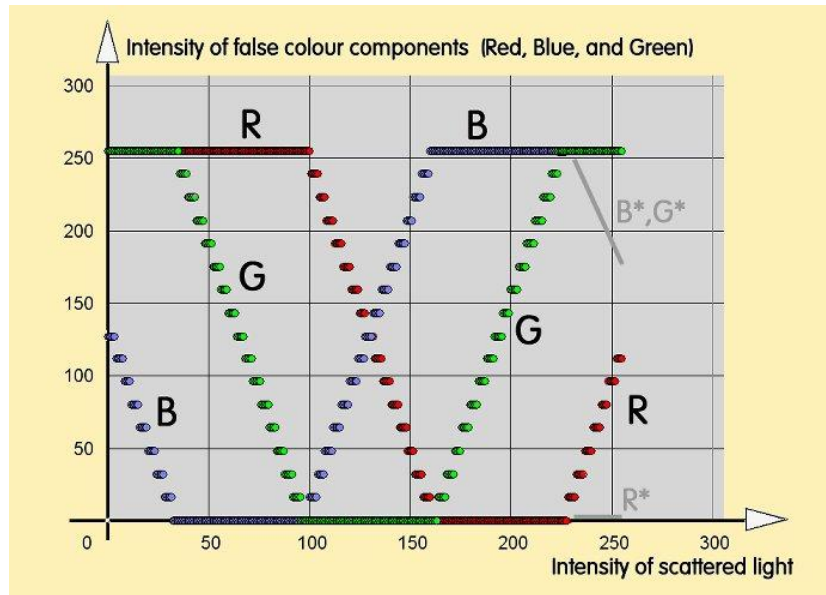
Fig. 4   Conversion diagram used for false-colour presentation grey-scale intensity images. It was used to obtain the images in Fig. 3. For symmetry of the function, the red component intensity R here rises at the blue end of the colourbar while B and G intensities remain high. A better appearance may be obtained with the suggested alternative, marked with asterisks.

presented in Fig. 4. The appearance of the red colour in Fig. 3, which shows a decrease of the scattered light intensity at the left-hand side of the images, is a consequence of the divergence of the laser light that illuminated the cross-sections from the right-hand side. Typically, the camera speed and picture storage capacity made it possible to obtain pictures at 5 deg phase interval at as many as 90 successive periods. In this case, if the images at a given phase were requested for phase averaging processing, they have to be extracted from the full file as those the sequential number of which differed by multiples of 360/5 = 72.

4. Image processing

In order to extract useful information from the images, they have to be processed. A number of existing methods is enormous [15], [16]. Currently the most popular method for identifying the structures from experimentally obtained visualisation images is the decomposition the flowfield into a "spectrum" of (linearly) superimposed components of increasing spatial complexity. It is expected that the essential features of the flow are revealed by the principal first-order component (or, at most, a few components of the lowest order). A typical representative of this approach is SVD, *singular value decomposition*, with its two special cases, BOD and POD. Our experience with this approach was presented in [3]. The methods are applied usually using a commercial software.

The fundamental assumptions of the decomposition methods are currently questioned — e.g., there are some inconsistences in the assumption on linearity of superpositions, the Gaussian character, the assumed importance of large variances, or the very basic feature of the orthogonality. From the point of view of detecting the
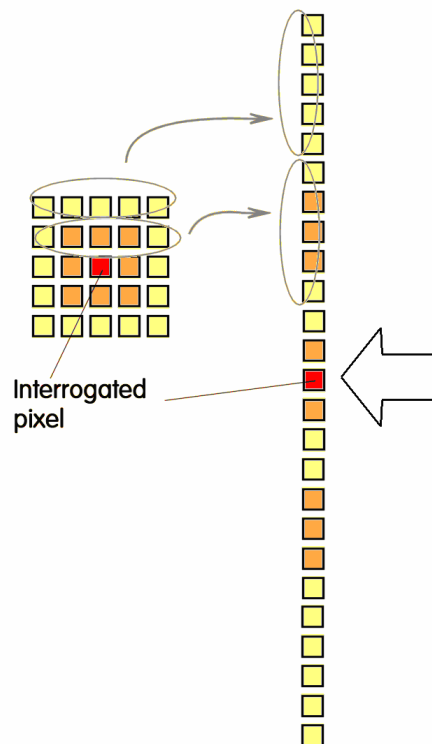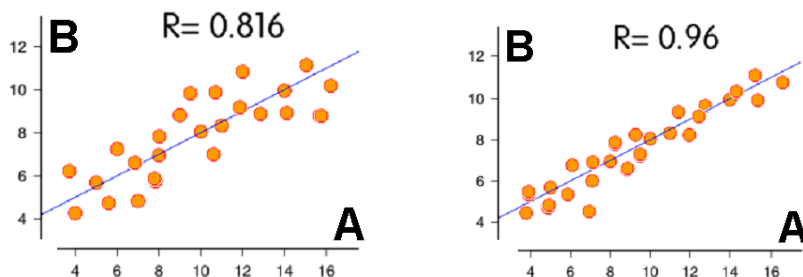
Fig. 5   The formation of the vectors A and B from the neighbouring pixels. Alternative choices are possible, whereby the procedure can either suppress or enhance some directions of motion in the interrogation plane..

Figs. 6, 7   Two examples of the correlation coefficients R computed for two 5 x 5 data values in the vectors A and B. The value R is interpreted as the measure of the scatter in the mutual linear dependence of the two vectors.

instability structures, it may be even questionable whether they are incorporated into the lower-order components of the "spectrum". Besides the prohibitive cost of commercial software packages, we have found as a limitation of the SVD variants for the present purpose of evaluating flow visualisation images their current practical implementations oriented exclusively to analysing PIV data with velocity information. This is missing in our currently available data.

Present authors   (Tesař and Něnička [17]) have developed another, very productive fully original approach for identification of the structures. It is based on the fact of the structures exhibit an increased measure of coherence in their movements. The

identification procedure consists of taking two flow visualisation images - separated by known time difference. The images containing no numerical information on velocities, only information about the local intensity of the scattered light. The pixels in one of the two images are then taken one by one and an interrogation vector **A** is evaluated from the greyscale intensity of the surrounding 5×5 pixels, as shown in Fig. 5, while an analogous vector **B** is formed by the same procedure from the neighbour pixels in the second image. Then this approach continues by computing the correlation coefficient R between the two vectors, **A** and **B** as

$$R = \frac{\overline{A \, B}}{|A||B|}$$

...(3)

(where the product in the numerator is the scalar vector product). The accompanying picture pair, Figs. 6 and 7, provides an example of graphical presentations of the mutual linear dependence of the two interrogation vectors. Both cases shown there are characterised by rather high values of the correlation coefficient R – in a flow with dominant chaos the values are generally lower. The value R thus evaluated according to eq. (3) between the two vectors, **A** and **B** is then presented in the image using a suitable colour coding.

The following Fig. 8 shows a typical example of the distribution of the values R in the plane of the cross section through the jet, with the colour coding information provided by the attached colourbar at the right-hand side. The green colour corresponds to regions of chaos, with zero or very low correlation coefficient value. There is no significant correlated motion inside the core of the jet. The red colour of higher correlation delineates the contours of the vortical motions. The same approach to the presentation is applied in the following Fig. 9. It presents, using the same colour coding,
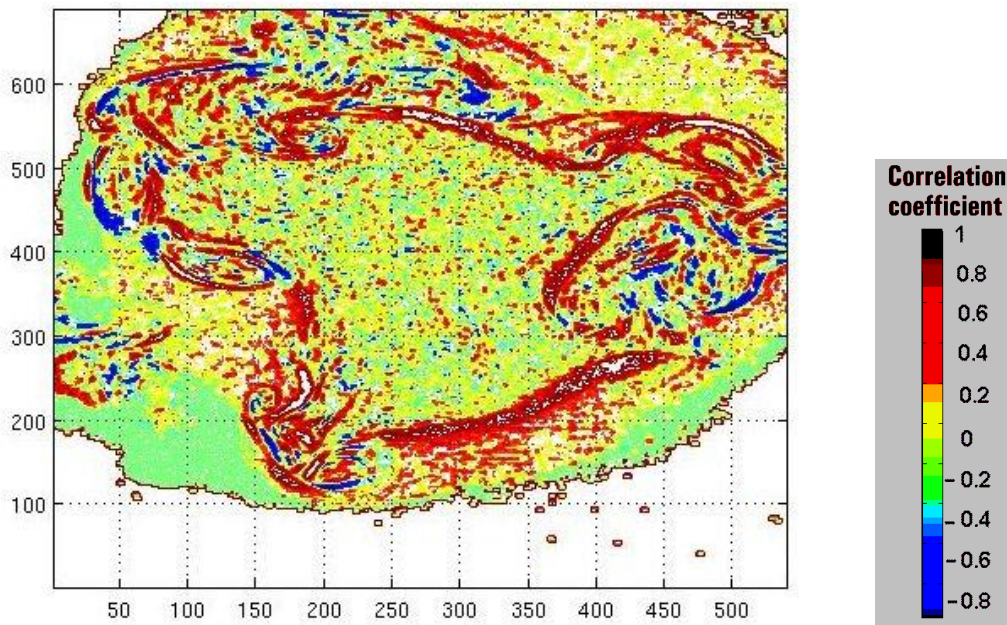

Fig. 8   An example of the cross-section image colour-coded by the local values of the magnitude of correlation coefficient evaluated for 5×5 sub-images. The red colour indicates the contours of vortical coherent structures. The absence of structures in the central part of the cross section is the consequence of the shear-less "potential" core of the jet.
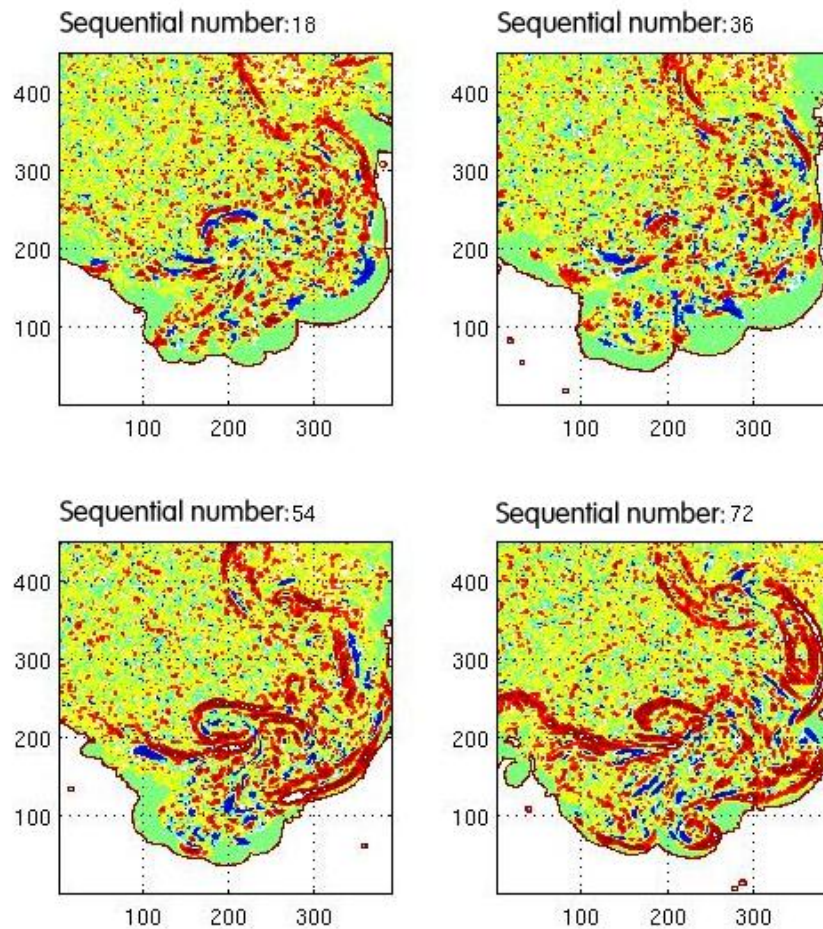
Fig. 9   A detail of an example of the jet cross section, evaluated in different phases of the harmonic excitation. The colour coding by the value of the correlation coefficient shows by the red colour of high R the boundaries of the interacting vortical object, seen in inclined cross sections. .

another example – concentrating on a detail at the bottom right periphery of the jet cross section. The images make possible to see of the boundaries of the coherent structures and, after some experience in interpretation is gained, also the character of mutual movements of the vortices. Unfortunately, the static illustrations as presented here cannot substitute the very much more convincing impression obtained if these images are used to form an animation.

Another useful image processing step making the vortical object and their movements in the interrogation plane more apparent is ***posterisation*** – a drastic reduction of the colour palette, leaving, e.g., only two colours. This simplified the image and makes clearly visible the relative motions, as presented in the following Figs. 10 and 11.

5. Theory of braiding movements

The problem of identification of the investigated vortical structures is closely associated with the problem of the mixing rate between the two fluids, as studied in the "static" mixers in microfluidics [30]. Various techniques were developed to measure the
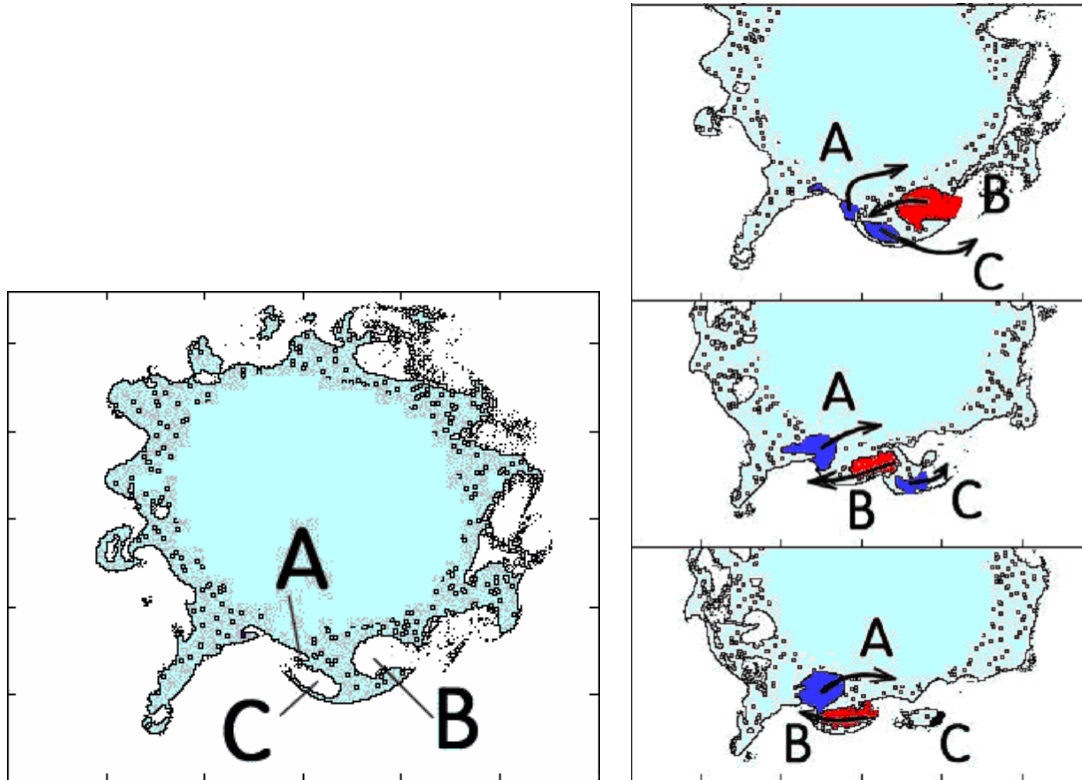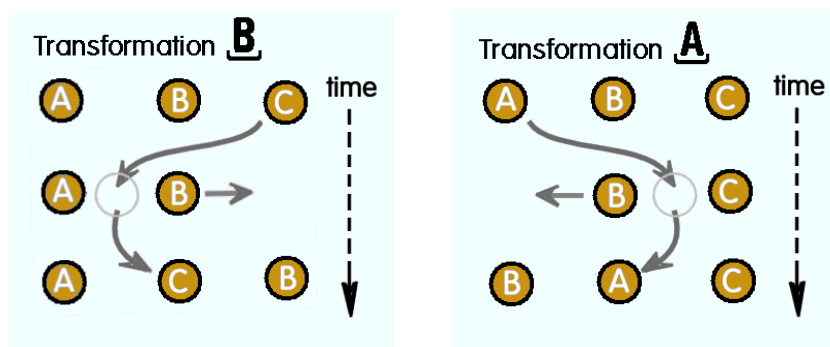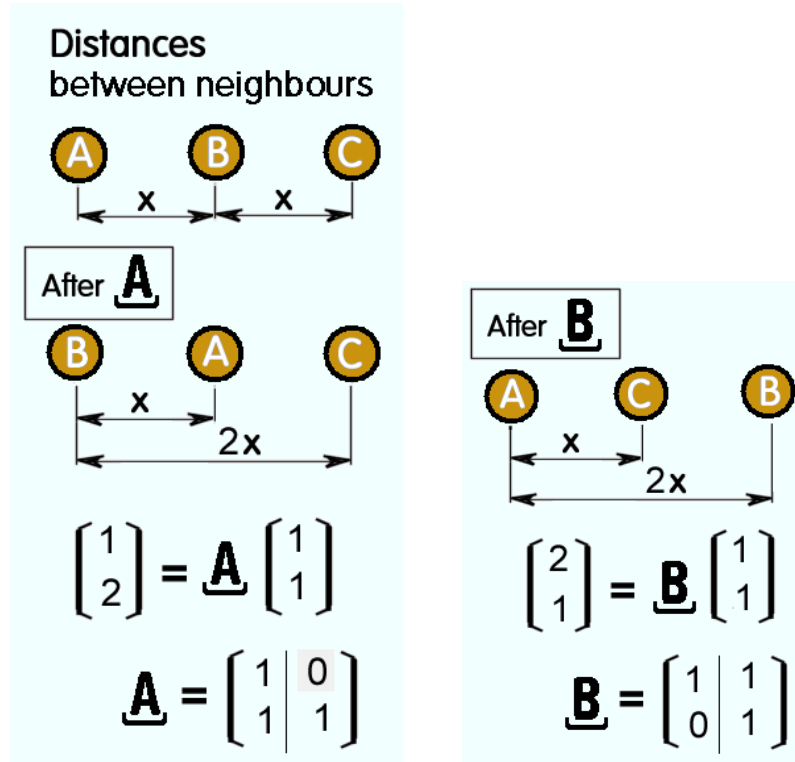
Fig. 10 (left): Typical boundaries evaluated by the posterisation procedure. The vortical objects are here presented as empty voids. **Fig. 11 (right)** The braiding motion of the vortices in the outer, mixing region of the jet, made more apparent by filling with blue and red colour. The pictures were taken after full 360 deg phase shifts..

mixing rate, such as the effective diffusion (e.g., Turner, Gilbert, and Thuburn [19], Shuckburgh and Haynes [20]) and the Lyapunov exponent (e.g., Wolf et al. [21], Pierrehumbert and Yang [22]).

One of the most advanced techniques is called "particle braiding" (Boyland, Aref, Stempler [23, 24], Kim and Sakajo [25], Turner and Berger [26]). To evaluate how chaotic is an investigated flow, this method measures the entanglement of particles and elongation of the distances between the fluid particles. Relative motions of the particles seen in a space-time diagram, produce a "braid" pattern, correlated with mixing and measured by the braiding exponent, equivalent to topological entropy. It is

Figs. 12, 13 Elements of the braiding transformation theory: positions of objects after two alternative braiding movements.

Distances between neighbours

After **A**

$$\begin{bmatrix} 1 \\ 2 \end{bmatrix} = \mathbf{A} \begin{bmatrix} 1 \\ 1 \end{bmatrix}$$

$$\mathbf{A} = \begin{bmatrix} 1 & 0 \\ 1 & 1 \end{bmatrix}$$

After **B**

$$\begin{bmatrix} 2 \\ 1 \end{bmatrix} = \mathbf{B} \begin{bmatrix} 1 \\ 1 \end{bmatrix}$$

$$\mathbf{B} = \begin{bmatrix} 1 & 1 \\ 0 & 1 \end{bmatrix}$$

Figs. 14, 15 Further element of the braiding theory: the distances between the objects after the unit braiding movements.

the lower bound of the rate of material lines stretching (Boyland, Aref, Stempler [23]) and is related to the Lyapunov exponent (Wolf et al. [21, Thiffeault and Finn [27]). The largest Lyapunov exponent provides the measure of the chaotic motion. Theory of the braiding motions is actually a mathematical group having two elements, Figs. 12, 13,
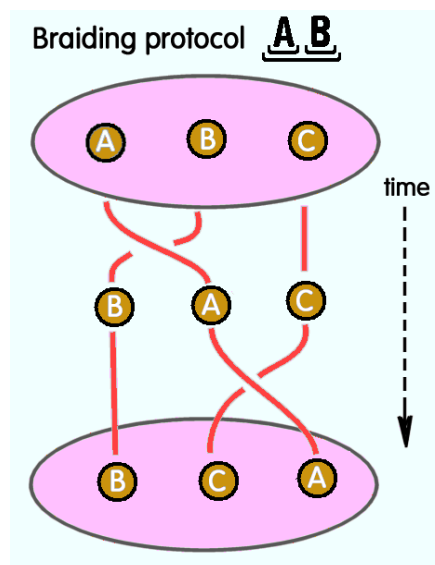
.

Braiding protocol A B

time

Fig. 16 Full braiding motion: the hair plait consists of objects positioned by repeated briding following the same protocol.
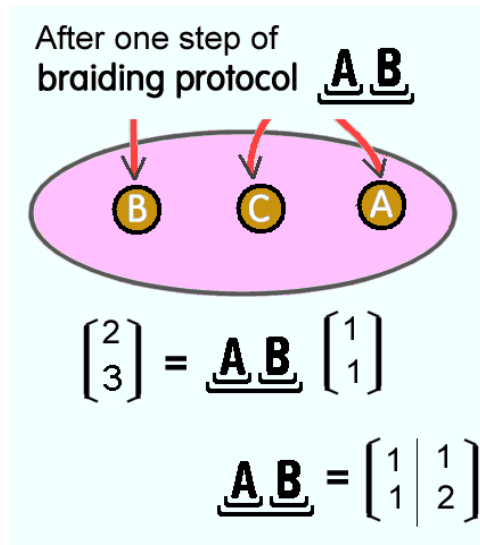
Fig. 17 Full braiding motion: the hair plait consists of objects positioned by repeated briding following the same protocol.

which may be represented by matrices that characterise the gradual increase of the distances between the objects as the repeated braiding motion progresses. The final lengths is obtained by the matrix product of all the matrices. The matrix associated with each of the transformations has unit eigenvalues. The matrix of the braiding protocol, however, has the larger eigenvalue 2.6180. This the distabnces between the original objects grows exponentially. This increase in the length of the vortices (which must keep its identities, as long as they are not overwhelmed by the turbulence) is the mechanism of transporting energy in the spectrum. Random matrix theory demonstrates that the largest aigenvalue of the final matrix product – the measure of the complexity of the braiding motion – grows exponentially. The rate of the exponential growth is the Lyapunov exponent.

References

[1] Tesař V., Trávníček Z.: " *Increasing Heat and/or Mass Transfer Rates in Impinging Jets*", Joural of Visualization, Vol. 8, No. 2, p. 91, 2005

[2] Tesař V.: "*The problem of off-axis transfer-effect extremes in impinging jets*", Proc. of XVIIth Internat. Scientific Conf. of Depts. of Fluid Mechanics and Thermomechanics, p. 187, Herlany, Slovakia, June 1998

[3] Tesař V., Uruba V., Něnička V.: "*PIV investigations of an excited air jet",* Proc. of Colloquium FLUID DYNAMICS 2010, p. 27, IT ASCR, October, 2010

[4] Tesař V., Něnička V.: "*Phase-Synchornised Investigations of Triggered Vortices in Impinging Jets*", Proc of "ENGINEERING MECHANICS 2009", p. 1321, Svratka, May 2009

[5] Tesař V., Něnička V., Šonský J., Kukačka L., Pavelka M.: "*Effect of Azimuthal Excitation in the Nozzle Exit on Structures Formed in Submerged Jets*", Proc. of Colloquium FLUID DYNAMICS 2008, Institute of Thermomechanics AS CR, v.v.i., Prague, October 2008

[6] Tesař V., Něnička V.: „*Study of Vortical Structures in Impinging Jets - New Methods and Approaches",* Proc. of ExHFT-7 the 7th World Conference on Experimental Heat Transfer, Fluid Mechanics and Thermodynamics, Krakow, Poland, 2009

[7] Tesař V.: "*Characterisation of subsonic axisymmetric nozzles*", Chemical Engineering Research and Design, p. 1253, Vol. 86, 2008

[8] Drobniak S., Klajny R.: "*Coherent Structures in Axisymetric Free Jets*", Journal of Turbulence, Vol. 3, p. 1, 2002

[9] Crow S. C., Champagne F. H.: "*Orderly Structure in Jet Turbulence*", Journal of Fluid Mechanics, Vol. 8, part 3, p. 547, 1971

[10] Brownand F.K,. Laufer J.: "*The Role of Large Scale Structures in the Submerged Jets*," Trans. ASCE, p. 1571, 1975

[11] Tesař V., Zimmerman W. B. J., Regunath G.: "*Helical Instability Structures in Swirling Jets*", Proc of the 8th International Symposium on Fluid Control, Measurements, and Visualization FLUCOME 2005, Chengdu, China, 2005

[12] Regunath G., et al.: "*Experimental investigation and visualization of helical structures in a novel swirling jet*", Proc. of FEDSM06, ASME Joint U.S. – European Fluids Engineering Summer Meeting, Miami FLA, July 2006

[13] Regunath G.S., et al. : "*Experimental investigation of helicity in turbulent swirling jet using dual-plane dye laser PIV technique*", Experiments in Fluids, ISSN 0723-4864, Springer Berlin/Heidelberg, Vol. 45, pp. 973-985, December 2008

[14] Moiseev S. S., Pungin V. G.: „*Analysis of Nonlinear Development of Helical Vortex Instability*", Fractals, Vol. 10, No. 4, p. 395, 2002

[15] Ottino J.M., et al.: „*Chaos, symmetry, and self-similarity: Exploiting order and disorder in mixing processes*", Science Vol. 257, p. 754, 1992

[16] Aubert G., Kornprobst P.: „*Mathematical problems in image processing*", Applied Mathematical Sciences 147, Springer, New York, 2006

[17] Tesař V., Němička V.: „*Processing Flow Visualisation Records by Correlation Coefficient Evaluation in Sub-Images*", Proc of "ENGINEERING MECHANICS 2010", Svratka, 2010

[15] Tesař V., Němička V., Šonský J.: "*Extracting Information About Coherence in Jet Flows*", Proc of "ENGINEERING MECHANICS 2009", p. 1333, Svratka, May 2009

[19] Turner M. R., Gilbert A. D., Thuburn J.:   „*Effective diffusion of scalar fields in a chaotic flow*", Phys. of Fluids, Vol. 20, p. 107103–1–14, 2008

[20] Shuckburgh E., Haynes P. H.   "*Diagnosing transport and mixing using a tracer-based coordinate system*" , Phys. of Fluids Vol. 15, p. 3342–57, 2003

[21] Wolf A. et al.: "*Determining Lyapunov exponents from a time series*", Physica, D 16 285–317

[22] Pierrehumbert R. T., Yang H.: " *Global chaotic mixing on isentropic surfaces*", Journ. of Atmos. Sci. Vol. 50, p. 2462–80, 1993

[23] Boyland P., Aref H., Stempler M. A.: "*Topogical fluid mechanics of stirring*", Journ. of Fluid Mechaniucs, Vol. 403, p. 277, 2000

[24] Boyland P., Stremler M., Aref H. : "*Topological fluid mechanics of point vortex motions*" Physica D **,** Vol. 175, p. 69, 2003

[25] Kin E., Sakajo T.: "*Efficient topological chaos embedded in the blinking vortex system*" Chaos , Vol. 15, p. 023111, 2005

[26] Turner M.R., Berger M.A.: "*A study of coherent vortices using braiding factors*", Fluid Dynam. Rsearch, Vol. 43, p. 035501, 2011

[27] Thiffeault J.-L., Finn M., "*Topology, Braids, and Mixing in Fluids*", Phil. Trans. Roy. Soc. A Vol. 364, p. 3251, 2006

[28] Pavelka M.: „*Posouvač fáze 25 - 250 Hz a generátor spouštěcího impulzu*" (Phase shifter 25 - 250 Hz and generator of triggering impulses – in Czech), Internal report, Institute of Thermomechanocs v.v.i., Academy of Sciences of the Czech Republic, 6 pages, 3 Figs., October 2007

[29] Tesař V., Něnička V.: "Instability Structures in Impinging-Jet Flows," *Proc. of International Conference EMT 2009 on Experimental Fluid Mechanics*, p. 335, Liberec, November 2009

[30] Tesař V.: " *Pressure-Driven Microfluidics*", monograph, Artech House Integrated Microsystems, Hardcover: 410 pages, Publisher: Artech House Publishers, Norwood, MA 02062 USA, 1 edition July 2007, ISBN-10: 1596931345, ISBN-13: 978-1596931343